J. Phys. B: At. Mol. Opt. Phys. **30** (1997) L697–L702. Printed in the UK PII: S0953-4075(97)86075-0

LETTER TO THE EDITOR

Charge transfer in C^{3+}–He^{2+} collisions

F Melchert†, S Meuser†, S Krüdener†, A Pfeiffer†, K v Diemar†, E Salzborn†, E Sidky‡ and C D Lin‡

† Institut für Kernphysik, Justus-Liebig-Universität Giessen, D-35392 Giessen, Germany
‡ J R Macdonald Laboratory, Department of Physics, Kansas State University, Manhattan, KS 66506, USA

Received 18 July 1997

Abstract. By means of a crossed-beams technique we have measured absolute cross sections for the charge-transfer reaction $C^{3+}+He^{2+} \rightarrow C^{4+}+He^{+}$ by coincident detection of the product ions C^{4+} and He^{+} for CM energies between 4 and 200 keV. Estimates of angular differential cross sections are made from measured scattering distributions of He^{+} reaction products at CM energies of 5.15 and 15.86 keV. The total cross sections for charge transfer are calculated by close coupling of a two-centre atomic basis.

Charge transfer in collisions between positive ions is an elementary process in all types of plasmas. In some circumstances ion–ion impacts may be competitive with electron impacts in determining the ionization structure, emissivity and energy loss from hot plasmas (see e.g. Baliunas and Butler 1980). Experimental data for ion–ion collisions required for various applications are sparse; for collisions between multiply charged ions they are practically absent.

Here we report absolute cross sections σ_C for the charge transfer process

$$^{13}C^{3+} + {}^{3}He^{2+} \rightarrow {}^{13}C^{4+} + {}^{3}He^{+} . \qquad (1)$$

The crossed-beams technique employed to investigate the above reaction was described in full detail previously (Meuser *et al* 1996). In short, the experimental arrangement consists of an ultra-high vacuum (UHV) chamber, a 'slow' and a 'fast' beamline. After momentum analysis, both ion beams are collimated by adjustable four-jaw slits to approximately 1.2 mm × 1.2 mm before they enter the UHV chamber. Shortly before intersection at an angle $\alpha = 17.5^{\circ}$, both ion beams are cleaned by electrostatic deflectors from particles in other charge states resulting from charge-changing collisions in the residual gas of the beamlines.

In the 'slow' beam C^{3+} ions are produced by a 5 GHz electron cyclotron resonance (ECR) ion source, analysed, focused and fed into the UHV interaction chamber. An electrostatic sector field with toroidal electrodes followed by a cylindrical condenser bends the beam towards the interaction volume where both ion beams cross. When a charge-exchange reaction occurs in an ion–ion collision, the reaction products have to be separated from the parent ion beams which are often 10^{12} times more intense. This task is fulfilled in both beamlines by two-stage units of electrostatic deflector plates in which one electrode of the second stage can be inclined to adjust the resolution to the actual requirements. C^{4+} reaction products are additionally deflected in a 180° hemispherical analyser and detected

0953-4075/97/200697+06$19.50

in a channeltron-based single-particle detector. The $^{13}C^{3+}$ isotope was chosen to avoid contamination of the primary beam by $^{4}He^{+}$ ions, which have virtually the same charge-to-mass ratio as $^{12}C^{3+}$ ions.

In the 'fast' beam He^{2+} ions are produced by a 2.45 GHz ECR ion source mounted on a high-voltage terminal. After acceleration, analysis and focusing the beam is bent by an electrostatic cylindrical condenser towards the interaction volume. The post-collision analysis is similar to that of the 'slow' beamline. For the measurement of absolute cross sections, He^{+} reaction products are detected in a channeltron-based single-particle detector. For position-resolved measurements, He^{+} ions are detected in a position-sensitive channel-plates detector. The $^{3}He^{2+}$ isotope was selected likewise to avoid contamination of the primary beam by molecular $^{1}H_{2}^{+}$ ions.

Although the crossed-beams technique, in principle, appears to be straightforward, inherent difficulties arise from the small target thickness provided by the ion beams. Even at ultra-high vacuum ($\sim 5 \times 10^{-11}$ mbar) in the interaction region, the residual gas density exceeds the ion densities within the beams. These conditions result in a comparatively low signal count rate (typically less than 1 count/s) and a poor signal-to-noise ratio (typically 10^{-4}). Therefore, a time coincidence technique is employed in order to distinguish between signal and noise events. The timing output pulses from the detector in the 'fast' beamline were fed, after amplification and discrimination, as a start pulse to a time-to-amplitude converter (TAC). The TAC is stopped by the output pulses of the detector in the 'slow' beamline. The time spectrum of the TAC output shows a well defined peak resulting from ion–ion reactions on top of a flat background due to random coincidences. The peak width is mainly determined by the finite length of the interaction volume.

The performance of the apparatus can be judged from typical experimental parameters of position-resolved cross section measurements listed in table 1 for two centre-of-mass (CM) energies. For the measurements of absolute cross sections, more intense primary beams with slightly larger diameters and divergences allowed for shorter data acquisition times.

Table 1. Typical experimental parameters of position-resolved cross section measurements for the reaction $C^{3+} + He^{2+} \rightarrow C^{4+} + He^{+}$ at CM energies $E_{CM} = 5.15$ and 15.86 keV. $E_{C^{3+}}$, $E_{He^{2+}}$, $I_{C^{3+}}$ and $I_{He^{2+}}$ denote the respective laboratory energies and currents of the C^{3+} and the He^{2+} ion beams, $N_{C^{4+}}$ and $N_{He^{+}}$ denote the respective detector count rates of the C^{4+} and the He^{+} reaction product ions. R, true coincidence signal rate; t, actual measurement time.

E_{CM} (keV)	$E_{C^{3+}}$ (keV)	$E_{He^{2+}}$ (keV)	$I_{C^{3+}}$ (nA)	$I_{He^{2+}}$ (nA)	$N_{C^{4+}}$ (s^{-1})	$N_{He^{+}}$ (s^{-1})	R (s^{-1})	t (h)
5.15	10.0	24.0	50	12	100	8000	0.07	22
15.86	10.0	47.0	60	15	150	1100	0.14	6

Measurements of absolute cross sections require correct measurements of beam intensities, beam energies, beam overlap and the complete detection of all reaction products. Several tests performed in order to ensure the proper function of the apparatus have been described elsewhere (Rinn *et al* 1985, Meuser *et al* 1996). Here, in particular, the complete detection of all He^{+} reaction products was ensured by use of a position-sensitive channel-plates detector in the 'fast' beamline. A measured scattering distribution of He^{+} ions originating from reaction (1) which gives an estimate of the angular scattering during a charge-changing ion–ion collision is shown in the left-hand part of figure 2 and will be

discussed in detail later. Due to the higher mass of the carbon ions, the 'crossed-beams' kinematics ensure much less angular scattering of C^{4+} ions produced in reaction (1) in the 'slow' beamline, where a channeltron-based single-particle detector was used. The minor importance of angular scattering in the 'slow' beamline was verified by 'flat-topped-peak' measurements for which the measured cross sections were found to be independent of the analyser voltages over a reasonable range.

Our measured total charge transfer cross sections σ_C are listed in table 2 with 90% confidence limits of random error. All cross sections are subject to an estimated additional uncertainty of $\pm 10\%$ resulting mainly from the error associated with the detection efficiency of the channel-plates detector.

Table 2. Measured and calculated cross sections σ_C for the charge transfer reaction $C^{3+} + He^{2+} \rightarrow C^{4+} + He^{+}$ for different centre-of-mass (CM) energies. The uncertainties of the measured data represent the 90% confidence limits of statistical error only.

	Measured cross section		Calculated cross section σ_C (10^{-16} cm^2)	
E_{CM} (keV)	σ_C (10^{-16} cm^2)	E_{CM} (keV)	Total	$He^+(1s)$ only
3.98	2.50 ± 0.21	2.4	2.61	2.45
4.99	2.50 ± 0.25	3.2	2.68	2.55
6.30	3.26 ± 0.27	4.8	2.87	2.76
7.94	3.20 ± 0.22	7.2	3.07	2.96
10.03	3.40 ± 0.28	9.6	3.29	3.15
12.59	3.83 ± 0.30	12.0	3.26	3.11
15.86	3.76 ± 0.28	14.4	3.27	3.11
19.95	3.44 ± 0.25	19.2	3.22	3.07
25.11	3.11 ± 0.25	24.0	3.06	2.91
31.59	2.95 ± 0.22	36.0	2.73	2.59
39.83	2.93 ± 0.24	48.0	2.44	2.27
50.14	2.46 ± 0.19	62.4	2.04	1.80
63.11	2.14 ± 0.18	79.2	1.72	1.38
79.50	2.09 ± 0.16	120.0	1.35	0.83
99.94	1.61 ± 0.14	160.8	1.08	0.55
125.9	1.40 ± 0.13			
158.6	1.43 ± 0.16			
199.5	1.06 ± 0.13			

The theoretical treatment assumes classical straight line trajectories for both ions, and expands the active electronic wavefunction as a sum of atomic states on both charge centres (Fritsch and Lin 1991). The effect of the two inner electrons of the lithium-like C^{3+} ion enters as a model screening potential for the outer electron

$$V_e(r) = [-Z_0 + (-Z_1 + \alpha r)\exp(-\alpha r)]/r \tag{2}$$

where $Z_0 = 4$, $Z_1 = 2$ and $\alpha = 2.47$. $Z_0 + Z_1$ is the bare nuclear charge, α is the screening parameter and Z_0 is the asymptotic charge of the C^{4+} ion. A total of 83 atomic states represent the electronic wavefunctions, including up to the $n = 4$ shell on both centres in addition to positive energy pseudo-states on the He^{2+} centre. The pseudo-states are not heavily populated after the collision, but they are included to improve the convergence of the expansion during the close collision.

In figure 1 we compare our measured cross sections with actual theoretical calculations. One can see that the measured and calculated total cross sections agree well to within the experimental error. Up to a collision energy of 50 keV the capture goes primarily into the $He^+(1s)$, since the $He^+(1s)$ energy level is closest to the initial C^{3+} binding energy. As one approaches the matching velocity, where the incoming alpha particle is travelling at about the average speed of the C^{3+} valence electron, the capture spreads to other states of He^+, and the 1s state represents only half the capture probability at 150 keV. At the high-energy impact (>120 keV) the capture probability was seen to vary by 25%, depending on which centre the pseudo-states were placed. However, the ratio of ground-state capture to excited-state capture remained the same.

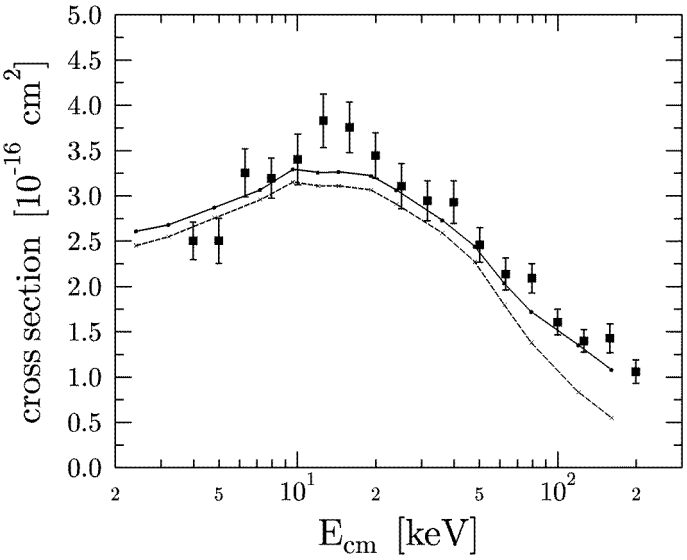

Figure 1. Charge transfer cross sections σ_C in the reaction $C^{3+} + He^{2+} \rightarrow C^{4+} + He^+$ with 90% confidence limits of random error. Full curve, present calculations; broken curve, present calculations, capture to $He^+(1s)$ final state only.

Measured scattering distributions of He^+ ions, recorded by the position-sensitive channel-plates detector, produced in ion–ion collisions (1) at $E_{CM} = 5.15$ keV and in collisions of He^{2+} ions with the residual gas (RG) at $E_{lab} = 24.0$ keV, are plotted in figure 2 on the left- and right-hand sides, respectively. Both spatial distributions were measured simultaneously and distinguished by application of a time-anticoincidence condition for the ion–RG distribution and a time-coincidence condition for the ion–ion distribution. Random coincidences were subtracted from the ion–ion distribution, which is plotted on a linear scale and contains 5250 events with a maximum of 12 counts/channel.

Extraction of angular differential cross sections from measured scattering distributions requires the transformation between the laboratory and the CM system as well as appropriate knowledge of the primary ion beam profile. The CM–laboratory transformation does not conserve rotational symmetry due to the crossed-beams kinematics. The primary ion beam profile (beam radius $r \approx 0.8$ mm, divergence half-angle $\Delta\alpha \approx 0.15^\circ$) broadens the observed scattering distribution and smears out structures. A deconvolution of the experimental data with respect to the primary ion beam profile is prevented by poor counting statistics. As a consequence, figure 3 shows apparent angular differential cross sections $(d\sigma/d\Omega)_{app}$

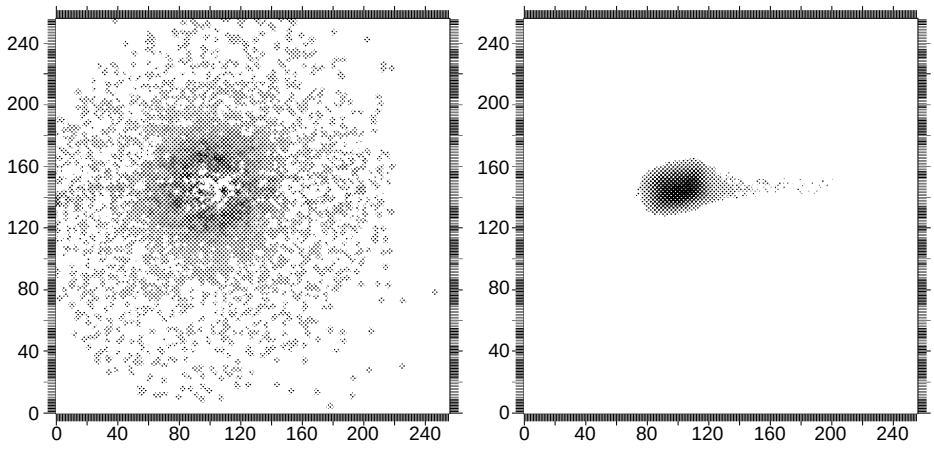

Figure 2. Measured scattering distributions of He^+ ions produced either in the reaction $C^{3+} + He^{2+} \rightarrow C^{4+} + He^+$ at $E_{CM} = 5.15$ keV (left) or in the reaction $He^{2+} + RG \rightarrow He^+ + \cdots$ at $E_{lab} = 24.0$ keV (right). RG denotes the residual gas in the UHV interaction chamber. The sensitive detector surface is divided in 256×256 channels corresponding to an area of 40×40 mm^2.

which result from convolution of $(d\sigma/d\Omega)$ with the primary ion beam profile. The cross section $(d\sigma/d\Omega)_{app}$ was obtained by transforming the measured scattering distributions from the laboratory frame to the CM frame and integrating over the azimuthal angle φ. For $E_{CM} = 5.15$ keV $(d\sigma/d\Omega)_{app}$ shows a dip in the forward direction ($\vartheta_{CM} = 0^\circ$) and peaks around $\vartheta_{CM} \approx 0.4^\circ$ with a FWHM of the distribution $(\vartheta_{CM})_{1/2} \approx 0.26^\circ$. For the higher kinetic energy $E_{CM} = 15.86$ keV no central dip of $(d\sigma/d\Omega)_{app}$ is evident. The apparent differential cross section drops to 50% of its maximum at scattering angles $\vartheta_{CM} \approx 0.24^\circ$. All these angles are smeared out by the finite experimental resolution originating mainly from the primary ion beam profile.

Convolution of the primary ion beam profile with the angular differential cross section for fast charge exchange collisions of He^{2+} ions with the residual gas (RG) yields the measured scattering distribution of He^+ ions for which the right-hand part of figure 2 is an example at $E_{lab} = 24.0$ keV. As the ion–RG cross section is not known, the measured ion–RG distribution is an upper limit for the primary ion beam profile. The FWHM of the ion–RG distribution, shown in the right-hand part of figure 2, is comparable to the size of the central dip in the ion–ion distribution, shown in the left-hand part of figure 2. Structure in figure 3 which occurs at CM scattering angles essentially smaller than the first maximum around $\vartheta_{CM} \approx 0.4^\circ$, may be caused by systematic errors of the measuring procedure.

Electron capture (3) of the 2s electron in the $^{13}C^{3+}$ ion into the 1s ground state of the $^3He^+$ ion requires $Q = -10$ eV of potential energy which is taken from the kinetic energy in the CM frame of the collision. If the capture populates a $^3He^+(2s)$ state, $Q = -51$ eV is needed:

$$^{13}C^{3+}(1s^2 2s) + {}^3He^{2+} \rightarrow {}^{13}C^{4+}(1s^2) + {}^3He^+(n\ell) + Q\,. \qquad (3)$$

The crossing of two ion beams defines an interaction plane. The kinematics yields a shift of the complete scattering distribution of ion–ion reaction products in the interaction plane with respect to the primary ion beam direction as a function of the Q-value. The primary ion beam direction is defined by the ion–residual gas scattering distribution, since the residual

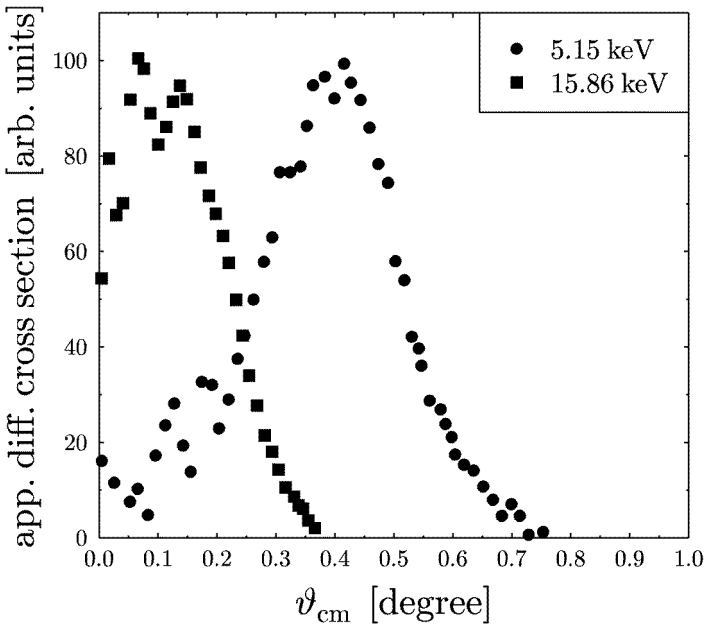

Figure 3. Apparent angular differential cross section $(\mathrm{d}\sigma/\mathrm{d}\Omega)_{\rm app}$ as a function of the CM scattering angle $\vartheta_{\rm CM}$ in the reaction $C^{3+} + He^{2+} \rightarrow C^{4+} + He^{+}$ at $E_{\rm CM} = 5.15$ keV (●) and $E_{\rm CM} = 15.86$ keV (■), respectively. The measured $(\mathrm{d}\sigma/\mathrm{d}\Omega)_{\rm app}$ is smeared out by the apparatus function which originates mainly from the finite width of the primary ion beam.

gas particles have random thermal velocities. Comparing both distributions in figure 2 by a projection perpendicular to the interaction plane, no shift in the interaction plane is observed to within an accuracy of (0.4 ± 2) channels which correspond to $Q = -(5.9 \pm 30)$ eV. From this finding, electron capture (3) to the 1s ground state of the He^{+} ion ($Q = -10$ eV) contributes mainly to the total cross section while capture to $n = 2$ ($Q = -51$ eV) or even higher states plays a minor role. The theoretical calculation described above confirms this experimental result.

The experimental part of this research was supported by BMFT under contract no 06-GI-333. The theoretical research was supported by the US Department of Energy, Office of Basic Energy Sciences, Division of Chemical Sciences.

References

Baliunas S L and Butler S E 1980 *Astrophys. J. Lett.* **235** L45–9
Fritsch W and Lin C D 1991 *Phys. Rep.* **202** 1–97
Meuser S, Melchert F, Krüdener S, Pfeiffer A, v Diemar K and Salzborn E 1996 *Rev. Sci. Instrum.* **67** 2752–9
Rinn K, Melchert F and Salzborn E 1985 *J. Phys. B: At. Mol. Phys.* **18** 3783–95